DISCOVERY OF NARROW X-RAY ABSORPTION LINES FROM NGC 3783 WITH THE *CHANDRA* HETGS

Shai Kaspi,[1] W. N. Brandt,[1] Hagai Netzer,[2] Rita Sambruna,[1] George Chartas,[1] Gordon P. Garmire,[1] and John A. Nousek[1]

2000 April 4, Accepted for publication in The Astrophysical Journal Letters

ABSTRACT

We present the first grating-resolution X-ray spectra of the Seyfert 1 galaxy NGC 3783, obtained with the High Energy Transmission Grating Spectrometer on the *Chandra* X-ray Observatory. These spectra reveal many narrow absorption lines from the H-like and He-like ions of O, Ne, Mg, Si, S and Ar, as well as Fe XVII–Fe XXI L-shell lines. We have also identified several weak emission lines, mainly from O and Ne. The absorption lines are blueshifted by a mean velocity of $\approx 440 \pm 200$ km s^{-1} and are not resolved, indicating a velocity dispersion within the absorbing gas of a few hundred km s^{-1} or less. We measure the lines' equivalent widths and compare them with the predictions of photoionization models. The best-fitting model has a microturbulence velocity of 150 km s^{-1} and a hydrogen column density of 1.3×10^{22} cm^{-2}. The measured blueshifts and inferred velocity dispersions of the X-ray absorption lines are consistent with those of the strongest UV absorption lines observed in this object. However, simple models that propose to strictly unify the X-ray and UV absorbers have difficulty explaining simultaneously the X-ray and UV absorption line strengths.

Subject headings: galaxies: active — galaxies: nuclei — galaxies: Seyfert — galaxies: individual (NGC 3783) — X-rays: galaxies — techniques: spectroscopic

1. INTRODUCTION

X-ray spectra of Active Galactic Nuclei (AGNs) often show evidence for deep O VII (739 eV) and O VIII (871 eV) absorption edges. The ionized gas component creating these edges is named the 'warm absorber' and is seen in most ($\gtrsim$70%) Seyfert 1s and some quasars. Theoretical models for the warm absorber suggest it should also be a source of X-ray emission (e.g., Netzer 1996) and absorption (e.g., Nicastro, Fiore, & Matt 1999) lines. While the current X-ray data are consistent with the presence of such lines (e.g., George et al 1998a), it has been impossible to study them in any detail.

The bright Seyfert 1 galaxy NGC 3783 ($V \approx 13.5$ mag, $z = 0.0097$) has one of the strongest X-ray warm absorbers known with a column density of ionized gas of $N_{\rm H} \approx (1\text{–}2)\times10^{22}$ cm^{-2}. *ASCA* spectra also show warm absorber variability and excess flux around 600 eV which has been interpreted as emission lines from the warm absorber, particularly O VII 568 eV (e.g., George et al. 1998a, 1998b). UV spectra of NGC 3783 show intrinsic absorption features due to C IV, N V and H I. Two kinematic absorption components are known with radial velocities of ≈ -560 km s^{-1} and ≈ -1420 km s^{-1} relative to the optical redshift from [O III]. The C IV absorption shows extreme variability (e.g., Crenshaw et al. 1999 and references therein). It is not clear whether the UV and X-ray absorbing gas are the same, although some relation seems likely (e.g., Shields & Hamann 1997).

This letter describes the discovery of a large number of X-ray absorption lines in the *Chandra* spectrum of NGC 3783. In § 2 we describe the observation and data analysis, and § 3 gives the preliminary interpretation of the results.

2. OBSERVATION AND DATA ANALYSIS

NGC 3783 was observed using the High Energy Transmission Grating Spectrometer (HETGS; C. R. Canizares et al., in preparation) on the *Chandra* X-ray Observatory[3] on 2000 January 21. The detector was the Advanced CCD Imaging Spectrometer (ACIS; G. P. Garmire et al., in preparation). The total integration time was 56 ks, and the observation was continuous. The data were reduced with the standard pipeline by the *Chandra* X-ray Center (CXC) on 2000 January 26. We used the *Chandra* Interactive Analysis of Observations (CIAO) software to repeat the reduction process using an updated response matrix file. Our reduction produced somewhat less noisy spectra than those produced by the pipeline.

The HETGS produces a zeroth order X-ray spectrum at the aim point on the CCD and higher order spectra which have much higher spectral resolution along the ACIS-S array. The higher order spectra are from two grating assemblies, the High Energy Grating (HEG) and Medium Energy Grating (MEG). Each grating assembly produces two spectra for each order. Order overlaps are discriminated by the intrinsic energy resolution of ACIS. The zeroth-order spectrum of NGC 3783 shows substantial photon pile up, and we leave the detailed analysis of these data to a future paper. We briefly comment, however, on the presence of a weak ($\approx$ 10 photon) off-nuclear ($\approx 34''$) source located at $\alpha_{2000} = 11^{\rm h}39^{\rm m}01\overset{\rm s}{.}1$, $\delta_{2000} = -37^\circ44'52\overset{''}{.}9$, coincident with one of the galaxy's spiral arms. This source may be a luminous ($L_{0.5\text{–}8\ {\rm keV}} \approx 2 \times 10^{39}$ ergs s^{-1}) X-ray binary in NGC 3783, although it could also be an unrelated background source.

The first-order spectra from the HEG and MEG have S/N ratios of ≈ 5 and ≈ 2.5, respectively (at around 7 Å). The higher

[1]Department of Astronomy and Astrophysics, 525 Davey Laboratory, The Pennsylvania State University, University Park, PA, 16802.
[2]School of Physics and Astronomy and the Wise Observatory, Raymond and Beverly Sackler Faculty of Exact Sciences, Tel-Aviv University, Tel-Aviv 69978, Israel.

[3]See *The Chandra Proposers' Observatory Guide* at http://asc.harvard.edu/udocs/docs/

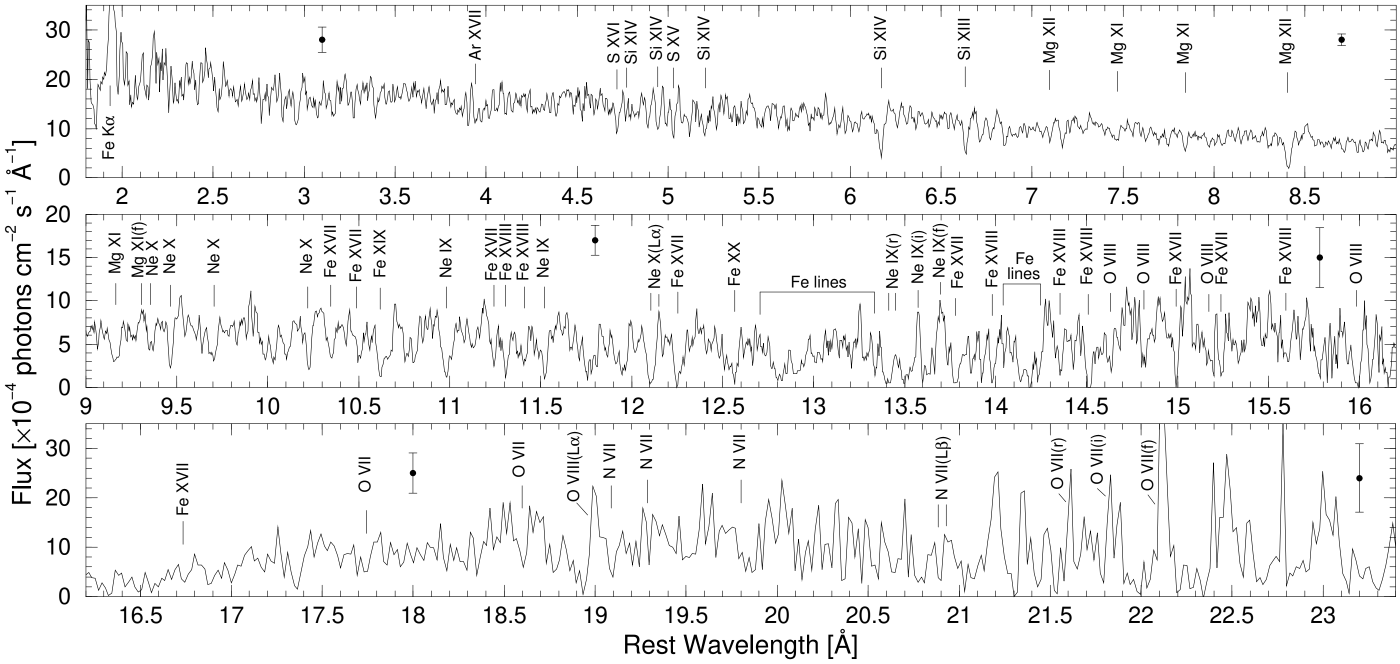

FIG. 1.— MEG first-order smoothed spectrum of NGC 3783. The two upper panels are binned by 0.005 Å, and the bottom panel is binned by 0.02 Å. Fluxes are corrected for Galactic absorption. Dots with error bars show the typical 2σ statistical error at various wavelengths. The identified absorption features are marked. The few identified emission lines are marked with (r) for resonance, (i) for intercombination, and (f) for forbidden for the He-like ions, as well as $L\alpha$ and $L\beta$ for the H-like ions.

order spectra had only a few (≈ 3) photons per bin and will not be presented here. In order to flux calibrate the spectra we used the CIAO software to produce Ancillary Response Files (ARFs). The flux calibration error is estimated to be $\lesssim 10\%$ below 6 Å and $\lesssim 20\%$ above 6 Å (CXC, private communication). We also corrected the spectra for the Galactic absorption of $N_{\rm H} = 8.7 \times 10^{20}$ cm^{-2} and the cosmological redshift.

The two MEG first-order spectra agree well with each other. The dispersions of the MEG spectra are 0.005 Å per bin, and the spectral resolution is ≈ 0.023 Å (approximately constant across the entire HETGS band). The two HEG spectra also agree well with each other and with the MEG spectra, though they have lower S/N. The HEG spectra have dispersions of 0.0025 Å per bin, and the spectral resolution is about two times better than for the MEG spectra. In Fig. 1 we present the mean of the two MEG spectra. This mean spectrum was smoothed using a simple 3-bin boxcar filter. Since above $\sim$16 Å there are $\lesssim 4$ counts per 0.005 Å bin, the spectrum presented in the bottom panel of Fig. 1 is binned to 0.02 Å.

The overall shape and flux of the X-ray spectrum are consistent with those found in previous X-ray observations of NGC 3783 (e.g., George et al. 1998b). The *Chandra* fluxes in several energy bands are also consistent with those from a simultaneous 4 ks *ASCA* spectrum to within $\approx 10\%$. The total flux measured from the *Chandra* spectrum is $(2.0\pm0.2)\times10^{-11}$ ergs cm^{-2} s^{-1} in the 0.5–2 keV band and $(4.2\pm0.9)\times10^{-11}$ ergs cm^{-2} s^{-1} in the 2–7 keV band. When plotting the modeled *ASCA* spectrum on top of the *Chandra* spectrum, we find general consistency in the overall shape as well as with the oxygen absorption edges.

The most striking new features seen in the *Chandra* spectrum of NGC 3783 are narrow X-ray absorption lines. In order to measure these spectral features we interpolated over all the absorption lines and fitted the resulting continuum with a cubic spline which serves as the continuum reference point for measuring the lines. In Table 1 we list the information about selected absorption and emission lines. In Fig. 1 we identify some absorption lines which are not listed in Table 1 due to brevity and lack of model predictions. There are also some absorption and emission features which appear to be present but are not identified yet. We used multiple lines from the same ion to help with line identification. We checked for the existence of these lines in each of the MEG spectra (and also in the HEG spectra when possible) and measured them in the smoothed average spectrum.

The measured lines' Full Widths at Half Maximum (FWHMs) are consistent with the MEG resolution which is ≈ 1300 km s^{-1} at 5 Å and ≈ 500 km s^{-1} at 15 Å. Hence, the lines are not clearly resolved (see discussion in § 3.2). We were not able to put better constraints on the velocity field with the HEG due to the small S/N.

3. DISCUSSION

3.1. *Absorption Lines, Column Density and Ionization Parameter*

The strongest observed absorption lines in the X-ray spectrum of NGC 3783 are from the H-like and He-like ions of O, Ne, Mg, Si, S and Ar, as well as Fe XVII–Fe XXI L-shell lines (see Table 1 but note that some features represent blends, and the values given are the summed EWs).

As explained above, the lines are not resolved, and the only firm conclusion is that, given a Gaussian profile, their FWHMs do not exceed a few hundred km s^{-1}. Given this uncertainty, we have taken an approach that relies solely on the measured EWs of the lines. We assumed a certain microturbulence velocity in a single line-of-sight cloud and calculated a theoretical spectrum with the photoionization code ION99, the 1999 version of the

TABLE 1
ABSORPTION AND EMISSION LINES FROM NGC 3783

Ion	Predicted λ (Å)	Velocity Shift (km s^{-1})	Predicted EW (mÅ)	Measured EW (mÅ)
Absorption Lines				
S XVI	4.728	–571±317	0.7	8.0±2.6
S XV	5.039	–535±297	8.2	7.5±2.5
Si XIV	5.217	–920±287	1.4	10.1±3.5
Si XIV	6.181	–534±242	7.7	17.3±4.6
Si XIII	6.648	–586±225	18.4	14.7±4.8
Mg XII	7.106	–379±211	6.6	6.2±2.2
Mg XI	7.473	–280±200	8.6	8.0±3.6
Mg XI	7.851	–382±191	15.6	9.7±3.1
Mg XII[a]	8.420	–463±178	>19.9	25.6±6.6
Mg XI[a]	9.170	–261±163	>25.9	34.5±10.2
Ne X	9.362	–384±320	6.2	16.4±4.5
Ne X[b]	9.481	–474±158	12.0	18.6±4.9
Ne X[a]	9.709	–216±154	>15.7	29.7±8.2
Ne X[a]	10.239	–410±146	>24.7	19.8±5.5
Ne IX[a]	11.001	–518±190	>20.1	50.4±12.2
Fe XVII	11.250	–186±133	23.3	15.7±4.3
Fe XVIII[a]	11.435	–629±131	>20.5	21.0±14.2
Ne IX[a]	11.547	–701±129	>49.3	27.2±7.4
Ne X[b]	12.132	–667±123	69.8	49.2±19.8
Fe XVII[b]	12.263	–391±122	43.1	51.9±12.8
O VIII	14.635	–20±102	34.3	24.8±12.2
O VIII	14.821	–182±101	38.9	27.8±12.8
O VIII	15.176	–79±197	42.8	35.8±11.2
Fe XVII	15.264	–471±196	42.7	30.6±8.4
Fe XVIII	15.628	–624±249	18.2	27.7±7.9
O VIII[a]	16.007	–346±121	>52.3	43.9±14.2
O VII	18.628	–515±322	52.1	41.9±14.8
N VII	19.120	–510±109	11.2	18.8±6.8
Emission Lines				
Mg XII	9.300	306±225	15	11.0±6.8
Ne X	12.132	444±123	36	44±24
Ne IX	13.447	64±111	19	99±88
Ne IX	13.553	464±110	13	163±140
Ne IX	13.699	26±175	41	245±215
O VIII	18.967	415±126	460	335±310
N VII	20.912	161±100	28	118±92
O VII	21.602	54±69	99	197±169
O VII	21.807	229±68	52	135±109
O VII	22.102	154±67	201	631±583

[a]Blended with Fe absorption lines which are not taken into account in the model.
[b]Blended with Fe absorption lines which are taken into account in the model.

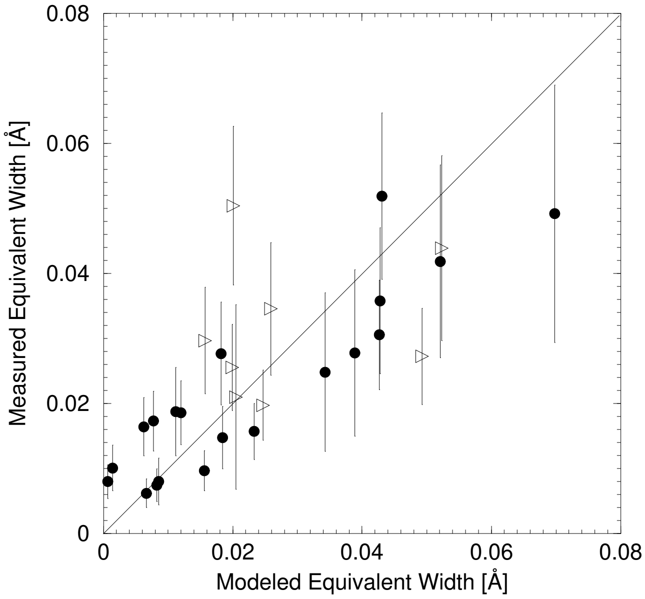

FIG. 2.— Measured versus modeled absorption line EWs. Filled circles are model EWs that are a sum of all lines contributing to the blend. Right-pointing triangles are lower limits for model EWs (see § 2 for details). The agreement between the model and the measured points is noticeable (Spearman rank-order correlation probability of $\approx 10^{-6}$). A line with a slope of unity is drawn to guide the eye.

TABLE 2
BEST MODEL COLUMN DENSITIES

Ion	Column (10^{17} cm^{-2})	Ion	Column (10^{17} cm^{-2})
O VII	5.0	S XVI	0.05
O VIII	38	Ar XVII	0.06
Ne IX	4.0	Ar XVIII	0.003
Ne X	6.9	Fe XVII	1.2
Mg XI	2.5	Fe XVIII	1.5
Mg XII	1.5	Fe XIX	1.0
Si XIII	2.2	Fe XX	0.4
Si XIV	0.5	Fe XXI	0.07
S XV	0.5	Fe XXII	0.02
C IV	2.4×10^{-5}	N V	4.7×10^{-4}

code ION (Netzer 1996). We then compared the results with the observations. The most important ingredients of the modelare the microturbulence velocity, the column density, the spectral energy distribution (SED), the ionization parameter, and the gas composition.

The atomic data required for calculating line optical depths are taken from various sources. The oscillator strengths for the H-like and He-like transitions of all metals are well known (e.g., Porquet & Dubau 2000 and references therein). This is not the case for the various iron L-shell lines where there is no standard published data set. In this paper we rely on various publications (e.g., Mason et al. 1979; Bhatia & Mason 1980; Cornille et al. 1992, 1994; Phillips et al. 1996; Saba et al. 1999) as well as on the National Institute of Standards and Technology (NIST) data set. These were combined with the Phillips et al. (1999) line lists, which are based on solar X-ray spectra and served as our major source for the wavelengths of the iron lines. Only 3–5 of the strongest iron lines, per ion, have been used in the analysis.

Our models are based on those in George et al. (1998b) that gave satisfactory fits to the 1993 and 1996 *ASCA* observations of the source. They include a weak UV-bump AGN SED (the weak IR case in Netzer 1996) with $\Gamma_{0.1-50\ \mathrm{keV}}$=1.75, a single constant density cloud with $N_{\mathrm{H}} = 1.3 \times 10^{22}$ cm^{-2}, solar composition, and a 0.1–10 keV ionization parameter of $U_{\mathrm{x}} = 0.13$. The standard ($E > 13.6$ eV) ionization parameter for this continuum is 19.3 and the mean temperature is 1.9×10^5 K. We have assumed Doppler profiles with $V^2 = V^2_{\mathrm{thermal}} + V^2_{\mathrm{turbulence}}$ and calculated absorption EWs for $100 < V_{\mathrm{turbulence}} < 600$ km s^{-1}. The best agreement with observations is for $V_{\mathrm{turbulence}}$=150 km s^{-1}. The model EWs are tabulated in Table 1. For a few lines we list only the model's EW lower-limit since the measurement includes blends for which we do not yet have a modeled EW. In most cases, the blends are expected to increase the modeled EW by $\approx$ 10–20%. The comparison between the observed and calculated EWs is shown in Fig. 2, and the deduced column densities, for the ions producing the strongest lines, are given in Table 2. All of the strong lines predicted by the model are observed in the spectra. The microturbulence velocity of our best fitted model is consistent with the velocity dispersion of the UV absorption lines (161±22 km s^{-1}; Crenshaw et al. 1999).

We have carried out basic tests to verify that the deduced line widths are in the right range. If the 'true' widths are much larger than assumed, the resonance lines in the H-like and He-like series will be optically thin. The observed EWs show that this is not the case. On the other hand, if the 'true' line widths are much smaller than 150 km s^{-1}, several of these lines will be saturated, giving very similar EWs to all. This is not observed either. While these are not strong conclusions given the S/N of the observations, it is encouraging to see the good agreement between the observed and calculated EWs, suggesting that the line optical depths are indeed in the intermediate range. According to the model, the largest optical depth for a line with $E > 1$ keV is τ(Ne X 12.132 Å)=35.

3.2. *Dynamics of the Absorbing Gas*

All the identified absorption lines in the HETG spectrum of NGC 3783 are blueshifted by a few hundred km s^{-1} with respect to the systemic velocity. The unweighted mean blueshift is 440±200 km s^{-1}. Kaastra et al. (2000) have recently observed the bright Seyfert 1 NGC 5548 using the Low Energy Transmission Grating Spectrometer (LETGS) on *Chandra*. The low-energy X-ray lines reported in that paper indicate a similar level of ionization, and the absorption lines are blueshifted by similar amounts. Judging by these first two results, it seems that the warm X-ray material in Seyfert 1 galaxies is outflowing with typical velocities of several hundred km s^{-1}. This has important implications for the dynamics of the absorbing gas as well as for the X-ray-UV connection.

The acceleration of X-ray ionized gas by the strong central radiation source in AGN has not been studied in detail so far (for some discussion see Reynolds & Fabian 1995). The recent work by Chelouche & Netzer (2000) is the first detailed study of this kind. This study discusses the motion of discrete, X-ray ionized clouds in hydrostatic equilibrium, under a large range of conditions. It shows that acceleration to velocities of a few hundred to a few thousand km s^{-1} is a natural consequence of the AGN environment. The terminal velocity is of the same order as the escape velocity in the region where the flow originates. Using these results, and assuming that the conditions in the nucleus of NGC 3783 are similar to those considered by Chelouche & Netzer (2000), we conclude that the origin of the warm absorbing gas in this source is outside the Broad Line Region, where the escape velocity drops below ≈ 1000 km s^{-1}. Better line profile analysis will enable us to constrain this location more accurately.

Another important comparison is with the UV absorption lines observed from this source. Several papers (e.g., Mathur, Elvis, & Wilkes 1995; Shields & Hamann 1997 and references therein) suggest that the UV and X-ray absorbers may originate in the same component. The Crenshaw et al. (1999) observations reveal two UV absorption systems, the strongest of which has a velocity consistent with the mean observed velocity of the X-ray gas and a velocity dispersion consistent with our best fitted model. Our model, which depends on the assumed SED, predicts column densities for C IV and N V (see Table 2) which are 37 and 5 times smaller, respectively, than what has been calculated by Crenshaw et al. (1999) using the 1993–1995 data. Hence the UV absorption lines appear to be inconsistent with our X-ray absorber model and are likely coming from a separate component.

3.3. *Emission Lines and Covering Factor*

The HETG spectra of NGC 3783 revel several weak emission lines (see Table 1) some of which show hints of P Cygni profiles. These have a marginally significant redshift with an unweighted mean of 230±170 km s^{-1} relative to the systemic velocity measured from the [O III] line. Kaastra et al. (2000) found similar redshifts for the emission lines in the LETG spectrum of NGC 5548. While the EWs of some of the lines are well within the MEG and HEG capability, the low S/N and bumpy continuum do not allow reliable EW measurements. The values given in Table 1 are therefore highly uncertain. However, even these rough measurements are good enough to test the idea that the central source in NGC 3783 is surrounded by gas clouds with properties similar to those deduced for the line-of-sight absorber. This is done by comparing the EWs calculated by ION with those observed, for various assumed covering factors.

The calculated emission-line EWs, for an assumed geometry of full covering, are listed in Table 1. Given these values, we find that the mean deduced covering factor is close to unity, in agreement with previous estimates (e.g., George et al. 1998b). This is the *first direct constraint* on the covering factor of a warm absorber in any AGN. Unfortunately, the uncertainty on the covering factor is large, due to the uncertain EWs. Further discussion of this issue, as well as detailed analysis of the continuum, emission features, and absorption features, are deferred to a future paper.

We thank all the members of the *Chandra* team for their enormous efforts. We also thank Herman L. Marshall and an anonymous referee for helpful comments. We gratefully acknowledge the financial support of NASA grant NAS 8-38252 (G. P. G., PI), NASA LTSA grant NAG 5-8107 (S. K., W. N. B.), and the Alfred P. Sloan Foundation (W. N. B.). H. N. acknowledges support from the Israel Science Foundation and the Jack Adler Chair for Extragalactic Astronomy.

REFERENCES

Bhatia, A. K., & Mason, H. E. 1980, A&A, 83, 380
Chelouche, D., & Netzer, H. 2000, ApJ, Submitted
Cornille, M., Dubau, J., Loulergue, M., Bely-Dubau, F., & Faucher, P. 1992, A&A, 259, 669
Cornille, M., Dubau, J., Faucher, P., Bely-Dubau, F., & Blancard, C. 1994, A&AS, 105, 77
Crenshaw, D. M. , Kraemer, S. B., Boggess, A. , Maran, S. P., Mushotzky, R. F., & Wu, C. -C. 1999, ApJ, 516, 750
George, I. M., Turner, T. J., Netzer, H. , Nandra, K., Mushotzky, R. F., & Yaqoob, T. 1998a, ApJS, 114, 73
George, I. M., Turner, T. J., Mushotzky, R., Nandra, K., & Netzer, H. 1998b, ApJ, 503, 174
Kaastra, J. S., Mewe, R., Liedahl, D. A., Komossa, S., & Brinkman, A. C. 2000, A&A, 354, L83
Mason, H. E., Doschek, G. A., Feldman, U., & Bhatia, A. K. 1979, A&A, 73, 74
Mathur, S., Elvis, M., & Wilkes, B. 1995, ApJ, 452, 230
Netzer, H. 1996, ApJ, 473, 781
Nicastro, F., Fiore, F., & Matt, G. 1999, ApJ, 517, 108
Phillips, K. J. H., Bhatia, A. K., Mason, H. E., & Zarro, D. M. 1996, ApJ, 466, 549
Phillips, K. J. H., Mewe, R., Harra-Murnion, L. K., Kaastra, J. S., Beiersdorfer, P., Brown, G. V., & Liedahl, D. A. 1999, ApJS, 138, 381
Porquet, D., & Dubau, J. 2000, A&AS, in press (astro-ph/0002319)
Reynolds, C. S., & Fabian, A. C. 1995, MNRAS, 273, 1167
Saba, J. L. R., Schmelz, J. T., Bhatia, A. K., & Strong, K. T. 1999, ApJ, 510, 1064
Shields, J. C., & Hamann, F. 1997, ApJ, 481, 752